Rev.Adv.Mater.Sci. 5 (2003) 121-133

PROCESSING OF NANOSCALE MATERIALS

R. G. Reddy

Center for Green Manufacturing, Department of Metallurgical and Materials Engineering, The University of Alabama, Tuscaloosa, AL 35487-0202, USA

Received: June 23, 2003

Abstract. Nanoscale materials can be processed by several techniques such as rapid solidification, plasma processing, *in-situ* chemical reaction, chemical vapor deposition, high energy ball milling, sol-gel method, *etc. In-situ* processing of nanomaterials has immense potential over the conventional nanoscale materials due to several advantages such as inherent chemical stability, lack of impurities, and fine dispersion. This paper deals with the thermal plasma technique in producing nanoscale metal, ceramic and composite powders and the various process parameters that influence the final product. Magnesium metal powders, ceramic powders such as SiC, B_4C, TiC and TiN, and composite powders such as Al-SiC, Fe-TiC, Fe-TiN have been successfully synthesized in our plasma processing laboratory. In this paper, the results of the synthesis of various powders are presented in detail.

1. INTRODUCTION

The powder metallurgical processing route is a useful approach for producing a wide range of developmental and commercial materials for various industrial applications. Different techniques like gas atomization, water atomization, centrifugal atomization, plasma atomization, mechanical attrition and alloying, melt spinning, rotating electrode process (REP), and a wide variety of chemical processes are used to produce metal powders [1]. These processes are described in the flow sheet shown in Fig. 1 and also in Table 1 [2]. High purity metal powders (Ti, Ni, Fe, Co, Cu, Mo, Al, Mg, Zr) and alloy powders (Ti-Al, Fe-Gd, Al-20Si, Nickel super alloys IN 100 and IN 718, 1018 Steel) have been successfully synthesized using various techniques as shown in the flow diagram in Fig. 1. Table 1 lists the different techniques used by various researchers in producing the metal/alloy powders. The type of powders produced along with their size ranges are also listed in the table [3-12].

Nanocomposites are a new class of structural materials where strengthening is achieved at the nanometer scale. Due to their nanometer size feature, nanocomposites exhibit markedly improved properties over conventional monolithic metallic alloys. Apart from the low density, these properties include improved strength, stiffness, wear resistance, and fatigue resistance, lower ductility and toughness. Although low density is one of the major benefits offered by nanocomposites, substitution of MMCs is not sufficiently cost-effective in many applications. Hence, the challenge is not only to improve the quality of discontinuously reinforced MMCs but also the cost of large scale production. Recent experimental studies [13-15] have noted the influence of particle size on the fatigue feature of particle–reinforced MMCs. Hence, the decrement of particle size to nanosize range improves the yield strength of composites as is shown in Fig. 2. It can be seen that significant improvement in mechanical properties of composites could be achieved with ceramic particles in the range of 1000 nm or less.

A major problem in processing nanoscale ceramic powders such as TiC, SiC, TiN, AlN with the state of the present technology is the existence of agglomerates in fine particles mainly due to high specific surface area [16]. Furthermore, segregation or inhomogeneous distribution of reinforcement

Corresponding author: R.G. Reddy, e-mail: rreddy@coe.eng.ua.edu

Fig. 1. Different processes for powder production.

particles and their agglomerates during solidification cannot be avoided because of the density difference between the metal or alloy and the reinforcement particles. However, in the thermal plasma processing of metal matrix composites, the high enthalpy of thermal plasma is used in vaporizing the raw materials rather than melting as in the case of plasma-sprayed deposition or plasma-sprayed coating. Thus, the reinforcing phase in the nanoscale gets homogeneously nucleated from the gas phase during shock quenching. These nanoscale reinforcement particles act as heterogeneous nucleation sites for the nucleation of the metal phase because of its very high surface activity and strong adherence. The formed metal phase grows and traps the nanoscale ceramic particles. The ceramic particles produced in this method can be encapsulated by a subsequent sintering process thus producing metal matrix composites with maximum dispersion of reinforcements. The reduction and/or elimination of interstitial volume can improve the strength of *in-situ* produced composites. Fig. 3 shows a schematic diagram of the whole process of producing and sintering nanocomposites in comparison with the conventional technique [14].

Fine powders such as borides, carbides, nitrides, inter-metallic compounds and composites have been successfully synthesized by thermal plasma processing. Formation of uniformly dispersed nanocomposites from gas phase requires control of nucleation and growth kinetics of the two competitive phases. Initially, the nucleation-controlled dispersed ceramic phase should form followed by the matrix phase. The matrix phase needs to be growth controlled in order to impart high interfacial growth rate which is required for trapping the dispersed ceramic phase. At the plasma operating temperature, the particle grows in a very short residence time resulting in a very uniform size of nanocomposites. With successful adoption of this strategy, our preliminary work [14] showed that *in-situ* processing of equilibrium nanoscale compos-

ites and other value-added materials was feasible by means of thermal plasma processing technique.

2. THERMAL PLASMA PROCESSING OF MATERIALS

Plasma processing of composites combines various processes, like heating, melting, quenching, and consolidation of fine particles (metallic or ceramic) into a single step. This is achieved by injecting the feed starting materials into a plasma reactor. Within the plasma reactor, the particles are rapidly heated, melted and simultaneously accelerated by the high velocity of hot gas. Plasma processing technique offers useful advantages in the synthesis of refractory materials, which require high temperatures and an impurity-free environment. The high heating and cooling rates in these systems allow the production of materials in certain metastable phases, which would be difficult by conventional processes. Synthesis of refractory materials by plasma includes the production of nano-meter size, material densification, and spheroidization of the ceramic powders. Hence, the main feature of the plasma processing technology is the controlled atmosphere at atmospheric pressure which is of prime importance for new application materials to produce high quality materials. Table 2 lists the various ceramic powders synthesized using thermal plasma processing technique by several researchers [17-23]. Several ceramic powders such as SiC, TiC, TiN, TiB_2, VC, ZrC, Si_3N_4 have been successfully produced by using D.C. arc plasma source. The precursors or raw materials and the plasma gas used in producing the respective powders are also given in the table along with the size ranges of products obtained for the systems.

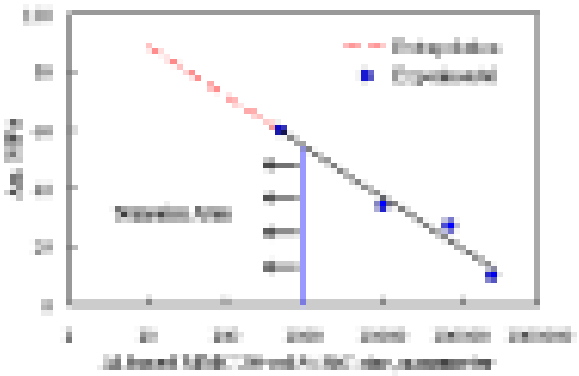

Fig. 2. Effect of reinforcement particle size on the yield strength of Al-based MMC-20% SiC.

The supersaturation condition of vapor species provides the driving force for particle condensation which leads to the production of ultrafine particles by homogeneous nucleation. The process of synthesizing ultrafine powders by a thermal plasma reactor includes the following stages: (i) injection of the reactants into the plasma reactor to overcome the high viscosity and the magnetic-hydrodynamic characteristics of the plasma; (ii) the feeding powders are heated, melted, vaporized, and dissociated into gaseous species; (iii) the gaseous species react with the feeding gas to form new compound and ultrafine particles by homogeneous nucleation and growth of the condensed species; and (iv) these particles and product gas undergo rapid quenching. Hence, the plasma processing is very suitable for producing refractory materials, such as metal car-

Table 1. Diameters of various powders produced by different techniques [2].

Process	*Product diameter (μm)*	*Powder produced*	*Reference*
Gas atomization	60-125	Nickel super alloy (IN 100), Ti, Zr, Ti-Al, Fe-Gd, Zn and Pb.	3, 4
Water atomization	12-16	Fe and Cu	4, 6
Centrifugal atomization	7-8	Al-20Si	7
Plasma atomization	40-90	Ti, Mo, Cu and IN 718 (Nickel superalloy)	8, 9
Plasma-rotating electrode process	75-200	1018 steel	10
Stamp mill, Ball mill	25-500	Al, Cu	4
Oxide reduction	1-10	Fe, Co, Cu, Mo, Al and Mg	4, 5
Carbonyl reactions	10	Fe, Ni	4, 12
Hydrometallurgical techniques	1-10	Ni	11

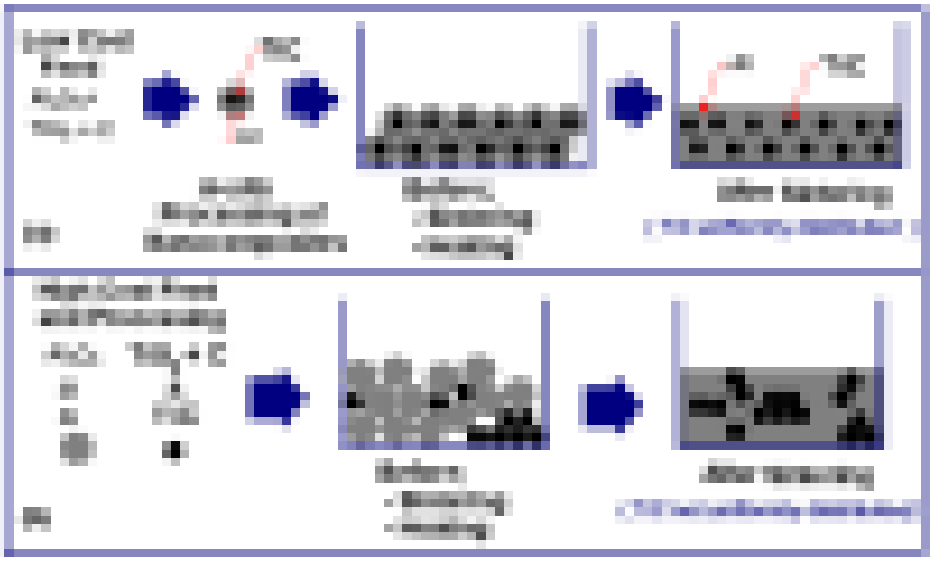

Fig. 3. Schematic comparison of (a) the present and (b) conventional techniques of producing nanocomposites in the metallic matrix.

bides and nitrides, commonly used as sintered compacts for high temperature applications.

Thermodynamics

The study of the application of MMCs at high-temperatures requires thorough understanding of both thermodynamics and kinetics of the system. Thermodynamic phase equilibrium data can contribute to identify the reinforcement materials that are stable in the metal-composite interface, whereas the reaction kinetic data can estimate the rate of the reaction at the interface. Thermodynamic equilibrium calculations can be performed using the Gibbs energy minimization method to determine the most stable composition of materials at different temperatures.

The Gibbs minimization method is based on the fact that the system will achieve the equilibrium condition at the lowest energy level. This is represented by Equation (1) [24]:

Table 2. Thermal Plasma Synthesis of Various Powders.

Product	*Precursors*	*Plasma Gas*	*Reactor*	*Product Size (nm)*	*Reference*
SiC	SiO, CH_4	Ar, H_2	d.c.	2-40	19
SiC	$SiCl_4$, CH_4	Ar, H_2	d.c.	100	19
SiC	SiO_2, CH_4	Ar, H_2	d.c.	200-400	19
B_4C	B_2O_3, CH_4	Ar, H_2	d.c.	200-400	17
TiC	TiO_2, CH_4	Ar, He, H_2	d.c.	200-400	20, 23
TiC	TiO_2, CH_4	Ar	d.c.	10	20, 23
TiC	$FeTiO_3$, CH_4	Ar, N_2	d.c.	Submicron	20, 23
TiB_2	TiO_2, B_2O_3, CH_4	Ar, H_2	d.c.	20-100	18
TiB_2	$FeTiO_3$, B_2O_3, CH_4	Ar, N_2	d.c.	Submicron	18
VC	V_2O_5, CH_4	Ar	d.c.	10-30	18
TiN	$FeTiO_3$, CH_4, NH_3	Ar, H_2	d.c.	20-100	18
Si_3N_4	$SiCl_4$, NH_3	Ar, H_2	d.c.	20-100	21
Si_3N_4	$SiCl_4$, NH_3	Ar, H_2	Hybrid	10-30	21
ZrC	$ZrSiO_4$, CH_4	Ar, He	d.c.	30-80	22

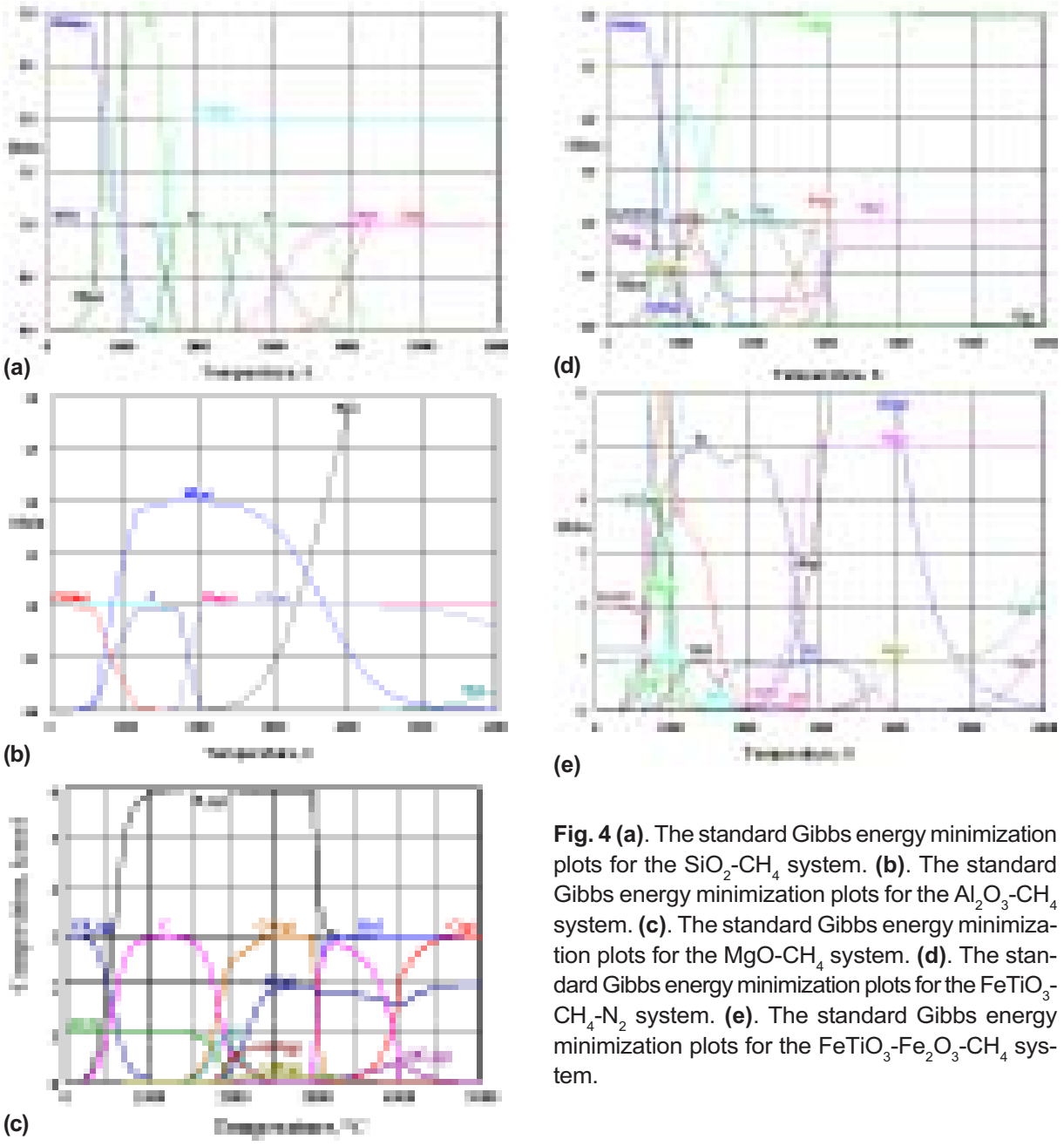

Fig. 4 (a). The standard Gibbs energy minimization plots for the SiO_2-CH_4 system. **(b)**. The standard Gibbs energy minimization plots for the Al_2O_3-CH_4 system. **(c)**. The standard Gibbs energy minimization plots for the MgO-CH_4 system. **(d)**. The standard Gibbs energy minimization plots for the $FeTiO_3$-CH_4-N_2 system. **(e)**. The standard Gibbs energy minimization plots for the $FeTiO_3$-Fe_2O_3-CH_4 system.

$$G = \sum_{gas} n_i (g_i^0 + \sum_{solution\,1} n_i (g_i^0 + RT \sum_{solution\,2} n_i (g_i^0 + RT \quad (1)$$

G is the total Gibbs energy of the system. g_i° is the standard molar Gibbs energy of species i at T and P. n_i is the number of moles of specie i, P_i is the partial pressure of specie i, and X_i and γ_i are the mole fraction and activity coefficient of specie i, respectively. n_i is the variable which minimize G and is subject to the mass balance constraint.

Calculation of Thermodynamic Properties

Thermodynamic calculations were performed for the process using a computer program HSC [25] based on the Gibbs energy minimization method [24] to determine the most stable compositions for the SiO_2-CH_4, MgO-CH_4, Al_2O_3-CH_4, $FeTiO_3$-CH_4-N_2 and $FeTiO_3$-Fe_2O_3-CH_4 systems as function of temperature. The ideal molar ratio for the process was de-

termined using HSC program [25]. Figs. 4(a)-4(e) show the Gibbs energy minimization plots for the respective systems. The overall chemical reaction for each system can be expressed as follows

$$SiO_2(s)+3CH_4(g)=SiC(s)+2CO(g)+6H_2(g), \quad (2)$$

$$MgO(s)+CH_4(g)=Mg(g)+CO(g)+2H_2(g), \quad (3)$$

$$Al_2O_3(s)+3CH_4(g)=2Al(g)+3CO(g)+6H_2(g), \quad (4)$$

$$FeTiO_3(s)+3CH_4(g)+0.75N_2(g) = Fe(s)+TiN(s)+6H_2(g)+3CO(g)+0.25N_2(g), \quad (5)$$

$$FeTiO_3(s)+2Fe_2O_3(s)+10CH_4(g) = TiC(s)+5Fe(s)+9CO(g)+20H_2(g). \quad (6)$$

Table 3 lists the temperature ranges for the equilibrium compositions of the product phases along with the molar ratios of the initial feed materials for the various systems studied in our laboratory. As an example, the equilibrium and distribution composition for the system Al_2O_3-TiO_2-CH_4 is shown in Fig. 5 as a function of temperature [26]. It can be seen that thermodynamically it is feasible to manufacture aluminum matrix nanocomposites reinforced with TiC by the thermal plasma processing technique. This is due to the rapid quenching of the vapor phase to temperatures below 3060 °C (melting point of TiC) that will lead to the condensation of TiC (reinforced phase). The homogeneously nucleated TiC particles of nanometer size, which have high surface area, will serve as heterogeneous nucleation sites for the condensation of aluminum phase at temperatures lower than 2500 °C, where the TiC phase is stable. Thus, nanoscale TiC particles will be encapsulated and distributed in the aluminum matrix.

Based on the stoichiometry of the respective systems, the feasibility of production of the desired products is determined from the above mentioned plots shown in Figs. 4(a)-4(e) and 5. The amounts

Table 3. Equilibrium compositions for various systems based on Gibbs energy minimization.

Product	*Precursors and their molar ratios*	*Temperature range, °C*
SiC	SiO_2:CH_4 = 1:3	1800-2200
Mg	MgO:CH_4 = 1:1	2000-2500
Al	Al_2O_3:CH_4 = 1:3	2500-3000
B4C	B_2O_3:CH_4 = 1:3.5	1600-2200
Fe-TiN	$FeTiO_3$:CH_4:N_2 = 1:3:0.75	1800-2200
Fe-TiC	$FeTiO_3$:Fe_2O_3:CH_4 = 1:2:10	2800-3500

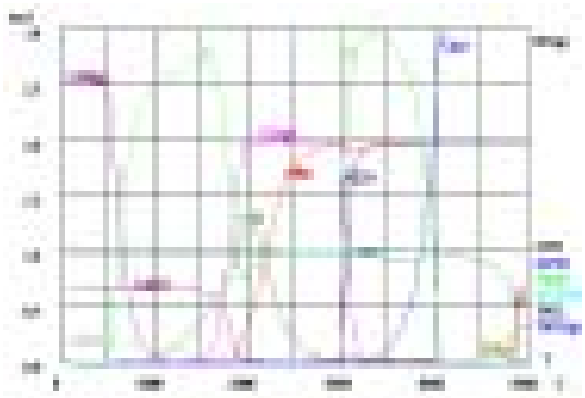

Fig. 5. The standard Gibbs energy minimization plots for the Al_2O_3-TiO_2-CH_4 system (molar ratio = 2:1:3).

of the various products that could be formed as a function of the reactants are analyzed in a relevant temperature range. Fig. 6(a) shows the equilibrium composition plot in the $FeTiO_3$-CH_4-N_2 system where the reactants $FeTiO_3$, CH_4 and N_2 are mixed in the ratio of 1:3:0.75. Fig. 6(b) shows the product compositions in the $FeTiO_3$-N_2 and $FeTiO_3$-CH_4 systems respectively. The plot shows the compositions of the reactants that need to be input inorder to obtain the desired products in the form of nanopowders for the Fe-TiN and Fe-TiC systems respectively.

Nucleation and Growth

Synthesis in a plasma reactor can be divided into different stages: (i) vaporization, (ii) chemical reaction, and (iii) condensation. In this condensation, nucleation (heterogeneous and homogenous) and growth phenomena takes place. Heterogeneous nucleation occurs under the existence of a third particle (either solid or liquid) and the nucleation rate depends greatly on the geometry and the chemical and physical surface properties of the pre-existing particles. On the other hand, homogeneous nucleation occurs when a stable condensed nucleus is formed from the supersaturated vapor and the particle grows randomly from the small condensed aggregates or clusters of the vapor molecules [27]. Hence, the particle formation process is considered to occur by the following events:

1. The gas phase reaction proceeds sufficiently until the saturation ratio exceeds a certain value.
2. The nucleation occurs like a burst over a relatively short time period (10^{-6} s).
3. The nucleation terminates due to the exhausted of nucleating species from the gas phase by diffusing to the recently formed particles.

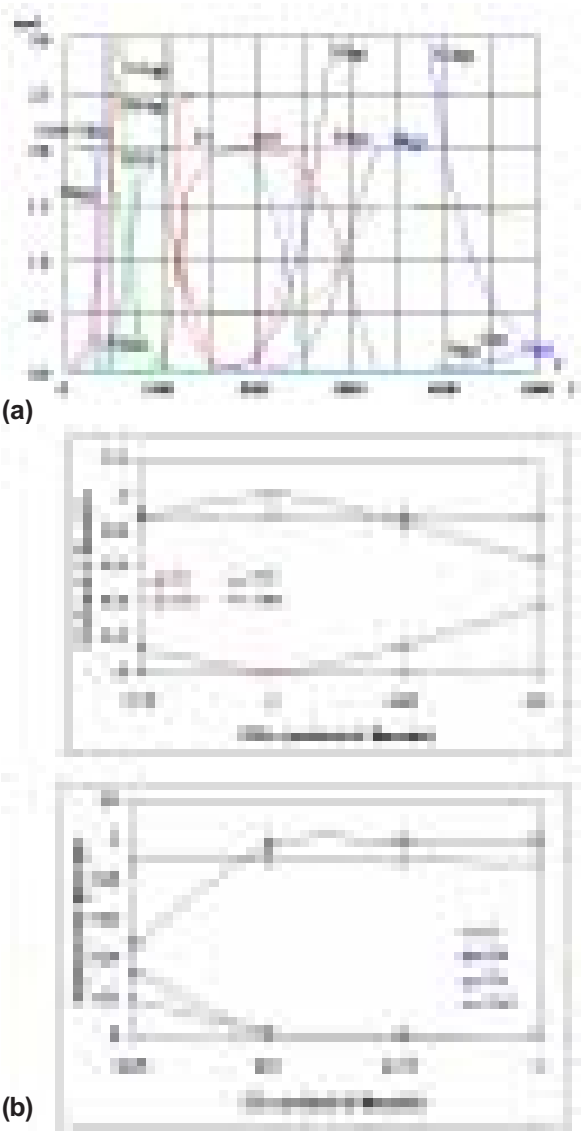

Fig. 6 (a). Equilibrium composition plot for the $FeTiO_3$-CH_4-N_2 system **(b)**. Product composition profile for the $FeTiO_3$-N_2 and $FeTiO_3$-CH_4 systems.

4. The particles continue to grow through physical condensation and coagulation with no formation of new particles.

Though heterogeneous nuclei usually occur, homogeneous nucleation is the prevailing mechanism for particle formation from the vapor phase, at least in the plasma processing where the residence time of particles are extremely short.

The minimum work (ΔG_t) required for forming a stationary spherical nucleus includes the energy for changing the volume of the particle and the energy for creating new surfaces and is given as:

$$\Delta G_t = \frac{4}{3}\pi r^3 \Delta G \qquad (7)$$

Eq. (7) describes the activation barrier, which must be overcome before the condensation process can proceed. Here, r is the nuclei radius, σ is the surface energy, and ΔG_V is the Gibbs energy per unit volume of liquid defined as:

$$\Delta G_V = -\left(\frac{kT}{v_l}\right)\ln \qquad (8)$$

S is the saturation ratio, v_l is the molecular volume of the liquid phase, and k is the Bolzmann's constant. From Eq. (7) a critical radius (r^*) can be derived after maximizing with respect to r:

$$r^* = \frac{-2\sigma}{\Delta G_V}. \qquad (9)$$

Therefore, the Gibbs energy change of formation of critical nucleus is,

$$\Delta G^* = \frac{16}{3}\frac{\pi\sigma^3}{\Delta G_V^2} \qquad (10)$$

while, the equilibrium concentration of nuclei of critical size r^* is,

$$n^* = n_s \exp\left(-\frac{}{}\right. \qquad (11)$$

n^* is the concentration of critical nuclei, and n_s is a function of P_e/kT, where P_e is the equilibrium vapor pressure of the condensing specie.

In a thermodynamic equilibrium of the concentration of critical nuclei with the vapor molecules, every collision among them will result in a stable nucleus. Hence, the equilibrium nucleation rate [27] is considered to be as:

$$J = A^* \omega n^* . \qquad (12)$$

A^* is a function of $4\pi r^{*2}$, and ω is the frequency of vapor molecules colliding per unit surface/unit time. Hence, J is giving as,

$$J = \alpha_c\left(4\pi r^{*2}\right)\left[\cdot\right. \qquad . \ (13)$$

α_c is the condensation coefficient, and m is the mass of molecular vapor.

The Gibbs energy of formation of a nucleus plays a similar role to that of the activation energy in conventional chemical kinetic, while the activation energy is a constant in magnitude; the ΔG, in contrast, changes markedly with the saturation ratio [24]. On the other hand, for a high particle concen-

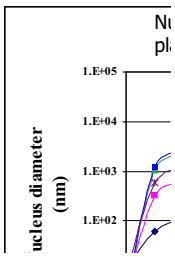

Fig. 7. TiN nucleus growth as a function of temperature and time.

tration and low saturation ratio, the condensation takes place on the existing particles without formation of new nuclei (heterogeneous condensation). Hence, the rate of condensation depends on the exchange of matter and heat between the particles and the continuous phase. The growth of the particle nucleus can be represented as [27]:

$$d_p = d_{p0} + \left[\frac{2v_l}{(2\tau} \quad . \qquad (14)$$

d_p is the particle diameter at time t, and d_{p0} is the particle diameter at $t = 0$.

Fig. 7 shows an example of the growth of a TiN nucleus considering Eq. (14) at different temperatures and times [14]. The shaded area A refers to the very short residence time of a particle in the plasma reactor.

3. *IN-SITU* PROCESSING OF FINE POWDERS

The production of fine powders is one of the major areas of development for the commercialization of thermal plasma arc systems. Due to very high temperatures that are attained in the plasma reactors, the rates of reactions are increased by several orders of magnitude [14]. Thus, this process is well suitable for the production of refractory materials, such as metal carbides and nitrides which are commonly used as cutting tool materials and as sintered compacts for high temperature structural materials. Using this novel technique, composites such as Fe-TiC, Fe-TiN, etc., have been manufactured with a unique microstructure. By adjusting the process parameters, it is possible to control the size distribution of the final product particles. We have worked on the thermal plasma synthesis of ultrafine particles and powders characterization, which may be metals, ceramics or composites [26,28-35]. Table 4 lists the various powders synthesized in our laboratory.

Synthesis of metal and ceramic powders

Some experiments were carried out to produce magnesium powders from MgO and graphite using non-transferred arc thermal plasma [33]. Fig. 8(a) shows the SEM micrograph of Mg/MgO product showing the evidence of shrinking core along with the corresponding XRD pattern of the powder product. Fig. 8(b) shows the effect of carbon content in the feed on the yield of magnesium powder produced by the thermal plasma processing technique. Recently, we have investigated the synthesis of SiC powders from SiO_2 and methane using the thermal plasma technique, and the preliminary results are very encouraging toward the production of nanosize SiC powders [30]. Fig. 9 shows SEM micrograph of the SiO_2-CH_4 system showing the final particles having a range of sizes (mostly sub-micron) and spherical in shape. XRD pattern of the particles is

Table 4. Operating conditions to produce various products by plasma processing technique.

Product	Precursors and their molar ratios	Power (kW)	Feed rate (g/min)	Reference
Fe-TiC	$FeTiO_3$:Fe_2O_3:CH_4 = 1:2:10	22.4	5.65	28
Fe-TiN	$FeTiO_3$:CH_4:N_2 = 1:3:0.75	22.4	2.28	28
Mg	MgO:CH_4 = 1:1	22.4	1.2	29
SiC	SiO_2:CH_4 = 1:3	25.5	6.6	30
B_4C	B_2O_3:CH_4 = 1:3.5	20.4	6.7	31
TiC	$FeTiO_3$:CH_4 = 1:4	20.4	4.0	26

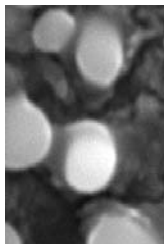

(a)

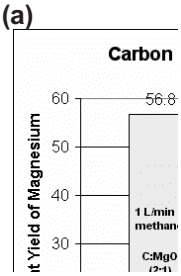

(b)

Fig. 8 (a). SEM micrograph of product Mg/MgO and the corresponding XRD pattern. **(b)**. Effect of carbon content in the feed on the yield of magnesium powder.

Fig. 9. SEM micrograph of SiC particles produced from SiO_2 and CH_4. XRD pattern of the powder is also seen.

also shown in the figure indicating that the product formed is indeed SiC with some carbon, which is probably due to the unreacted carbon from methane. However, further investigation is underway to standardize the system for the production of nanoscale SiC powders. The ultimate aim in this direction is to produce Al-SiC composite powders using alumina as the source for aluminum. Work is in progress to synthesize B_4C nanopowders from B_2O_3 and CH_4. Fig. 10 shows an SEM micrograph, EDX pattern of the marked B_4C particle, elemental analysis of the product particle and XRD pattern obtained in the B_2O_3-CH_4 system [31]. The results clearly indicate that fine B_4C powders were successfully synthesized. The particles were agglomerated, and the average size of individual particles is less than 100 nm. Fig. 11 shows the preliminary results obtained in the synthesis of TiC powders using ilmenite and methane. The particles labeled as a, b, c in the micrograph are in the size range of 80-200 nm [26].

Synthesis of composite powders.

Thermal plasma synthesis of iron-titanium carbide and iron-titanium nitride composites has been carried out in our plasma laboratory. The composites have been synthesized in-situ using the thermal plasma technology and the reinforced particles were

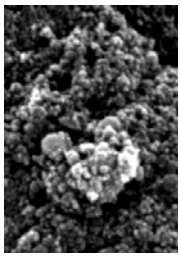

Fig. 10. SEM micrograph and XRD pattern of B_4C particles synthesized using B_2O_3 and CH_4.

in the nanoscale range. Fig. 12 shows the SEM micrographs at two different magnifications of homogeneously nucleated nanosize TiC particles in

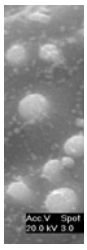

Fig. 12. SEM micrograph of powders in the Fe-TiC system at two different magnifications along with EDX spextra of the regions marked as (a) and (b) on the micrograph.

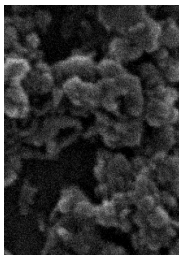

Fig. 11. SEM micrograph of TiC particles synthesized using Ilmenite powder and methane. The particles labeled as a, b, c are in the size range of 80-200 nm.

the Fe-TiC system produced from ilmenite and hematite feed. EDX spectra of the particles labeled as (a) and (b) in the micrograph are also shown in the figure. Spherical nanosized and well dispersed TiC particles are clearly seen in the micrograph. Experiments were carried out to synthesize Fe-TiN composites using the same technique with ilmenite as solid feed and a mixture of methane and nitrogen in appropriate proportions as reacting gaseous input to the plasma reactor. Fig. 13 shows the SEM micrograph of the cross-sectional area in the Fe-TiC composite where (a) is Fe-alloy and (b) is TiC. EDX spectra of the regions marked as (a) and (b) on the micrograph and XRD pattern of the Fe-TiC composite system are also shown in the figure.

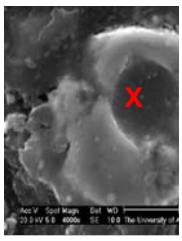

Fig. 13. SEM micrograph showing cross-sectional area of the Fe-TiC composite. EDX spectrum of the region marked as (X) on the micrograph and XRD pattern of the Fe-TiC composite system are also shown in the figure.

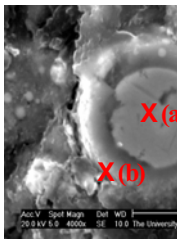

Fig. 14. SEM micrograph showing cross-sectional area of the Fe-TiN composite where (a) is Fe-alloy and (b) is TiN. EDX spectra of the regions marked as (a) and (b) on the micrograph and XRD pattern of the Fe-TiN composite system are also shown in the figure.

Fig. 14 shows the SEM micrograph, EDX patterns of the labeled regions (a) and (b) on the micrograph and also the XRD pattern of the Fe-TiN composite system. The nanoscale TiN particles are encapsulated in an iron-alloy matrix and are well distributed. The micrograph suggests a very unique structure for a composite powder particle produced in-situ via thermal plasma technology. The core of the sub-micron particle is composed of the ceramic material (TiN) whereas the outer layer around the ceramic particle is pure iron, thereby leading to a composite production with a well-defined and clean interface between the matrix and ceramic materials. Such a microstructure has not been reported earlier to this by this technique. The present investigation on iron based composite powders production will initiate a new technology for nanocomposites manufacture on a large scale with optimum properties of the final compacted composite.

Based on the results obtained in the synthesis of the composite powders for the Fe-TiC and Fe-TiN systems, recovery of the final ceramic product was plotted as a function of nitrogen content of the input gases in Fig. 15. It is very clear from the above figure that to obtain TiC alone in the final product we need to have methane alone as the reacting gas, whereas to produce TiN we can use methane along with nitrogen in appropriate ratios. Methane in the latter system acts as a reducing agent for oxygen in the system and will also protect from the reverse reaction of oxidation of iron and titanium. However,

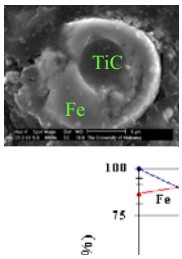

Fig. 15. TiN and TiC formation from ilmenite as a function of nitrogen gas.

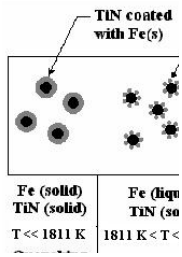

Fig. 16. Schematic diagram of plasma reactor showing the mechanism of *in-situ* formation of Fe-TiN composite powders.

here the methane percentage in the input gases needs close control in order to avoid the formation of TiC which can form if the input gas contains excess methane. Fig. 16 shows the schematic diagram of plasma reactor showing the mechanism of *in-situ* formation of Fe-TiN composite powders. Essentially, the schematic diagram depicts the regions in the reactor divided according to the temperature zones and the respective solidification sequence that takes place from the torch region to the quenching zone. Fig. 17 shows the schematic flow sheet of the various powders that were produced in our plasma laboratory. We have successfully synthesized fine metal, ceramic and composite powders in our plasma reactor. Research is being carried out to extend the present technology to produce other ceramic and composite powders and to optimize the process parameters so as to produce nanoscale products.

Fig.17. A schematic sketch showing different powders produced at the plasma processing laboratory.

4. CONCLUSIONS

Fine powders of Mg, SiC, TiC, TiN, B_4C, Fe-TiC, Fe-TiN and Al-SiC were successfully synthesized by the thermal plasma processing technique. The results obtained in this research clearly indicate that high purity nanoscale metal, ceramic and metal-ceramic composite powders could be synthesized by this technique. These results area a source of inspiration for the production of various nanocomposite powders and the subsequent testing of composites obtained by compacting these fine powders. Further investigations are underway to optimize the operating parameters for the production of nanoscale ceramic and composite powders.

ACKNOWLEDGEMENTS

The author is pleased to acknowledge Dr. Divakar Mantha for his help in reviewing the paper and the financial support for this research by the U.S Department of Defense (grant number DAAD 19-01-1-0137).

REFERENCES

[1] A. Alagheband and C. Brown // *Metal Powder Report* **53** (1998) 30.
[2] Leo V. M. Antony and R. G. Reddy // *JOM* **55** (2003) 14.
[3] M. Hohmann, W. Diemer, N. Ludwig and W. R. Zenker // *Advances in Powder Metallurgy* **1** (1992) 27.
[4] T. Yukimasa and S. Takemori // *Metallurgical Review of MMIJ* **6** (1989) 38.
[5] S. White, R.G. Reddy and B. Wu, In: *Light Metals 2000*, ed. By R. D. Peterson (Warrendale, PA, TMS 2000) p. 871.
[6] S. Okamato, T. Sawayama and Y. Seki // *Metal Powder Report* **51** (3) (1996) 28.
[7] S. Chen // *Trans. of Non-Ferrous Metals Society of China (English Edition)* **7** (1997) 12.
[8] Anon // *Metal Powder Report* **52** (1997) 34.
[9] S. Grenier // *Metal Powder Report* **53** (1998) 26.
[10] S. A. Miller, In: *Proceedings of the Advanced Particulate Materials and Processes* (West Palm Beach, FL, 1997) p. 457.
[11] M. A. Clegg and K. T. Horn // *Horizons of Powder Metallurgy* **1** (1986) 175.
[12] K. Iwai and H. Yasuda // *New Materials and New Processes* **3** (1985) 241.
[13] J. N. Hall, J. W. Jones and A. K. Sachdev // *Mater. Sci. Engg.* **A183** (1994) 69.
[14] R. G. Reddy // *Metall. Mater. Trans. B* **34B** (2003) 137.

[15] R. G. Reddy and B. Wu, *US Patent No. 6,343,640,* Feb 5, 2002.
[16] R. Vaßen and D. Stöver // *Journal of Materials Processing Technology* **92-93** (1999) 77.
[17] P. R. Taylor, A. Pirzada and G. L. Watt // In: *Proceedings of EPD congress 1994*, ed. by B. Mishra (TMS, Warrendale, PA, 1994), p. 941.
[18] S. Mitrofranov, A. Mazza and E.Pfender // *Mat. Sci. Engg.* **48** (1981) 21.
[19] P. R. Taylor and S. A. Pirzada // *Metall. Trans. B* **23B** (1992) 443.
[20] Ya-Li Li and Takamasa Ishigaki // *J. Amer. Ceram. Soc.* **84** (9) (2001) 1929.
[21] S. C. Danforth // *Nanostructured Materials* **1** (1992) 197.
[22] Z. G. Kostic, P. L. Stefanovic, P. B. Pavlovic, Z. N. Pavlovic and N. V. Pavlovic // *Ceramics International* **27** (2001) 547.
[23] P. R. Taylor, M. Manrique, S. A. Pirzada and M. Abdel-Latif // *Plasma Chemistry and Plasma Processing* **15** (3) (1995) 545.
[24] N. A. Gokcen and R. G. Reddy, *Thermodynamics* (Plenum Press, New York, 1996).
[25] A. Ronie, *HSC Chemistry*, Ver 4.1 (Outokumpu Research Oy, Pori, Finland, 2000).
[26] L. Tong and R. G. Reddy, *hermal Plasma Processing of Nanoscale TiC powders*, *Unpublished research*.
[27] S. K. Friedlander, *Smoke, Dust, and Haze: Fundamentals of Aerosol Dynamics*, (Oxford University Press, New York, 2000).
[28] S. Niyomwas, *hermal plasma in-situ processing of TiN and TiC reinforced Fe alloy ultrafine composites*, Ph.D. Dissertation, The University of Alabama, 2001.
[29] Z. Zhang and R. G. Reddy, *Unpublished research*, 2002.
[30] R.G. Reddy and Leo V. M. Antony // *JOM*, **55** (2003) 19.
[31] N. Thakkar and R. G. Reddy, *Thermal Plasma Synthesis of Boron Carbide Fine Powders*, *Unpublished research*, 2003.
[32] S. W. White and R. G. Reddy, In: Proceedings of EPD Congress, (TMS, 1999) p. 687.
[33] S. White, R.G. Reddy and B. Wu, In: *Light Metals 2000*, ed. by R.D Peterson, (2000) p. 871.
[34] S. Niyomwas, Banqiu Wu and R.G. Reddy In: *Materials Processing in the Computer Age III*, ed. by V.R. Voller *et al.*, (TMS, 2000) p.199.
[35] S. Niyomwas, B. Wu and R.G.Reddy, In: *Ultrafine Grained materials,* ed. by B.S. Mishra, S.L. Semiatin, C. Suryanarayana, N.N. Thandhani and T.C. Lowe (TMS, Warrendale, PA, 2000) p.89.